Impact of HVS Models on Model-Based Halftoning

Sang Ho Kim, *Student Member, IEEE,* and Jan P. Allebach, *Fellow, IEEE*

***Abstract*—A model for the human visual system (HVS) is an important component of many halftoning algorithms. Using the iterative direct binary search (DBS) algorithm, we compare the halftone texture quality provided by four different HVS models that have been reported in the literature. Choosing one HVS model as the best for DBS, we then develop an approximation to that model which significantly improves computational performance while minimally increasing the complexity of the code. By varying the parameters of this model, we find that it is possible to tune it to the gray level being rendered, and to thus yield superior halftone quality across the tone scale. We then develop a dual-metric DBS algorithm that effectively provides a tone-dependent HVS model without a large increase in computational complexity.**

***Index Terms*—Digital halftoning, error metrics, human visual system model, nonlinear optimization, printing.**

I. Introduction

HALFTONING is the process of rendering an image with a large set of possible pixel values into another image with a smaller set of pixel values for output devices with limited output levels such as printers and monitors. Halftoning relies on the fact that the human visual system acts as a low-pass filter; and thus it is possible to create an impression of shades of gray with an appropriate dot size and dot density.

Based on the type of computation involved, halftoning algorithms may be broadly classified into three categories: point processes, neighborhood processes, and iterative processes. Point processes include screening [1] and lookup table based algorithms [2], and only require a pixel-by-pixel comparison with a spatially varying threshold to determine the halftoned output value of the current pixel. On the other hand, error diffusion [3], which is a neighborhood process, compares the sum of the current pixel and weighted neighborhood errors with a threshold to determine the halftoned value. During the past 25 years, especially the last decade, a great deal of research has been directed toward improving the quality of screening and error diffusion. References [4] and [5] provide extensive reviews of this effort.

Iterative or search-based methods require several passes of processing to determine the final halftone image. These methods try to minimize the error between the continuous-tone image and the output halftone image by searching for the best possible configuration of the binary values in the halftone image. Iterative methods are the most computationally intensive of the three categories; but they yield significantly better output quality than screening or error diffusion.

In addition to their use to directly synthesize high-quality halftone images, iterative algorithms have played an important role in the development of point processes that yield better quality halftones than could be previously achieved, with the same level of computation [6]–[10]. Here, the level of computation refers to the effort required to transform a specific continuous-tone image to a bilevel halftone image, not the computation required to design the parameters of the halftoning algorithm.

Nearly all digital halftoning algorithms are either implicitly or explicitly based on a model for the human visual system (HVS) [11]. For example, Bayer's screen [1] is designed to push spectral energy in the halftone texture away from the origin to higher frequencies. Similarly the weights for Floyd-Steinberg error diffusion [3] have been shown to effectively process the diffused error with a low-pass filter. Finally, Ulichney's void and cluster algorithm [12] employs a Gaussian filter to determine the location of voids and clusters in the halftone texture. All these algorithms are consistent with a model that treats the HVS as a low-pass filter. However, since the HVS model is not an explicit part of these algorithms, we do not consider them to be model-based. In the following paragraph, we will review halftoning algorithms that do explicitly incorporate a model for the HVS, and which are thus model-based in the sense that we have defined it.

First, we consider screening algorithms. Sullivan *et al.* used simulated annealing for level-by-level design of a halftone screen [2], [13]. They minimized a cost function consisting of the frequency-weighted energy in the texture, where the frequency-weighting was based on a HVS model. Allebach and Lin used the direct binary search method to design both monochrome and color screens [7], [8]. Here, the cost function was also essentially frequency weighted mean squared error; but it was computed in the spatial domain. Under the category of error diffusion algorithms, Kolpatzik and Bouman employed a visual filter to optimize the weights [14], Sullivan *et al.* used visually filtered binary texture for error computation and threshold modulation [15], and Wong used a visual filter to adapt the weights as the image is binarized [16], [17]. Finally, we come to the applications to iterative halftone methods. Zakhor *et al.* employed a HVS weighting in conjunction with linear programming on a block-by-block basis to find a good halftone image [18]. Analoui and Allebach [19], Mulligan and Ahumada [20], and Pappas and Neuhoff [21] all used iterative search heuristics to minimize the mean squared error between the halftone and continuous-tone images, after filtering with the point spread function of a HVS model.

In this paper, we will consider exclusively a halftoning method called direct binary search (DBS) which is a visual

Manuscript received December 28, 2000; revised December 11, 2001. This research was supported by the Hewlett-Packard Company. The associate editor coordinating the review of this manuscript and approving it for publication was Prof. Robert L. Stevenson.

The authors are with the School of Electrical and Computer Engineering, Purdue University, West Lafayette, IN 47907-1285 (e-mail: kim11@ecn.purdue.edu; allebach@ecn.purdue.edu).

Publisher Item Identifier S 1057-7149(02)01728-1.

TABLE I
CONTRAST SENSITIVITY FUNCTIONS OF FIVE HVS MODELS FROM THE LITERATURE

Author	Contrast senstivity function $\bar{H}(\bar{\rho})$	Constants
Campbell	$k(e^{-2\pi\alpha\bar{\rho}} - e^{-2\pi\beta\bar{\rho}})$	$\alpha = 0.012,\ \beta = 0.046$
Mannos	$a(b + c\bar{\rho})\exp(-(c\bar{\rho})^d)$	$a = 2.6,\ b = 0.0192,$ $c = 0.114,\ d = 1.1$
Näsänen	$\exp(\frac{-\bar{\rho}}{c\log\frac{L}{}+d})$	$c = 0.525,\ d = 3.91,$ $L = 11$
Daly	$a(b + c\bar{\rho})\exp(-(c\bar{\rho})^d)\,, \quad \bar{\rho} > \bar{\rho}_{max},$ $1\,, \qquad\qquad\qquad\qquad \text{else.}$	$a = 2.2,\ b = 0.192,$ $c = 0.114,\ d = 1.1,$ $\bar{\rho}_{max} = 6.6$
Barten	$\frac{\sqrt{T/2}}{K}\frac{\exp(-\pi^2(\sigma_0^2+c_{sph}^2 d^6)\bar{\rho}^2)}{\sqrt{(1/(\eta pI)+\Phi_0/(1-\exp(-\bar{\rho}^2/\bar{\rho}_0^2))(1/X_0^2+1/X_e^2+\bar{\rho}^2/N_e^2)}}$	For parameters, refer to [30].

model-based and iterative halftoning method. For a review of this algorithm, the reader is directed to [19], [22], [23], and [24]. A brief overview of the DBS algorithm will be given in Section II-B.

Despite the advances that have been made during the past 25 years in modeling the human visual system [11], [25], the HVS models that have been incorporated in halftoning algorithms have been limited to linear shift-invariant filters based on the contrast sensitivity function (CSF) of the human viewer (Table I). A number of different CSFs have been reported in the literature [26]–[30]. We will review them briefly in Section III-A. To our knowledge, there has never been a systematic attempt to compare the effectiveness of these models in the context of digital halftoning. Such a comparison is the first goal of this paper. It will be the subject of Section III-B, and it will lead to our designation of one CSF model as the best for use with the DBS algorithm.

The second goal of the paper is to find an approximation to this CSF that will improve the computational efficiency of DBS without unduly increasing the complexity of the code. We will do this in Section IV. By varying the parameters of this approximating function, we will find that it is possible to tune the HVS model to yield better texture quality within a specific range of gray levels. This leads us to the third goal of the paper which is to develop a dual-metric form of the DBS algorithm that effectively provides a tone-dependent HVS model without sacrificing the computational efficiency of the standard DBS algorithm. This is the subject of Section V.

II. PRELIMINARIES

In this section, we will set up the relationship between the HVS/printer models and the halftoning algorithm. We will also introduce the concept of the scale parameter, which will be needed to establish the relationship between the printer resolution/viewing distance and the HVS model parameters. Finally, we will briefly describe the DBS algorithm which will serve as the basis for our new algorithm.

A. Printer and Visual Models and Scale Parameter

Throughout this paper, we will use $[m, n]$ and (x, y) to denote discrete and continuous spatial coordinates, respectively. The units of $[m, n]$ and (x, y) are pixels and inches, respectively. Let $f[m, n]$ be the continuous-tone image and $f(x, y)$ be the rendition of this continuous-tone image by an ideal printer. An ideal printer is one that can reproduce an ideal square pixel with absorptance equal to that of the continuous-tone pixel. Likewise, let $g[m, n] = 0$ or 1 represent the halftone image. Then, the following equations hold:

$$f(x, y) = \sum_{m,n} f[m, n]p(x - mX, y - nY) \tag{1}$$

$$g(x, y) = \sum_{m,n} g[m, n]p(x - mX, y - nY) \tag{2}$$

where $p(x, y) = \text{rect}(x/X, y/Y)$ is the dot rendering function of an ideal printer, and X and Y are the basis for the lattice of printer addressable dots in units of in/dot.

The HVS will be modeled as a linear shift invariant filter; and the point spread function (PSF) of the HVS will be denoted by $h(x, y)$. The perceived continuous-tone image is given by

$$\begin{aligned}\tilde{f}(x, y) &= f(x, y) ** h(x, y),\\ &= \sum_{m,n} f[m, n]\tilde{p}(x - mX, y - nY)\end{aligned} \tag{3}$$

where $**$ denotes two-dimensional (2-D) convolution and $\tilde{p}(x, y) = p(x, y) ** h(x, y)$ embodies the effects of cascading the printer rendering and HVS models.

Similarly, the perceived halftone image can be written as

$$\tilde{g}(x,y) = \sum_{m,n} g[m,n]\tilde{p}(x - mX, y - nY). \quad (4)$$

With a high-resolution device such as a 600 dpi laser printer, the printer dot profile $p(x,y)$ is sufficiently narrow compared to $h(x,y)$ so that $\tilde{p}(x,y) \approx h(x,y)$. Throughout this paper, we will assume that this relationship holds and refer to the HVS PSF as $\tilde{p}(x,y)$.

The HVS PSF $\tilde{p}(x,y)$ is based on the contrast sensitivity function (CSF) $\bar{H}(\bar{u},\bar{v})$ of the human visual system. Here, $(\bar{u},\bar{v})$ takes the units of cycles/degree subtended at the retina. Taking the inverse Fourier transform of $\bar{H}(\bar{u},\bar{v})$ yields the point spread function $\bar{h}(\bar{x},\bar{y})$, where $(\bar{x},\bar{y})$ has the dimensions of degrees subtended at the retina.

$$\bar{h}(\bar{x},\bar{y}) = \mathcal{F}^{-1}\{\bar{H}(\bar{u},\bar{v})\}. \quad (5)$$

To convert the angular units of the above equation to the units on the printed page, we note that a length x inches when viewed at a distance D inches will subtend an angle $\bar{x}$ degrees according to the relationship

$$\bar{x} = \frac{180}{\pi}\tan^{-1}\left(\frac{x}{D}\right) \approx \frac{180x}{\pi D}, \quad \text{for } x \ll D. \quad (6)$$

Similarly, the relationship between the angular frequency $\bar{u}$ in cycles/degree and the spatial frequency u in cycles/inch is given by $\bar{u} = \pi D u/180$. Thus,

$$\begin{aligned}\tilde{p}(x,y) = h(x,y) &= \frac{180^2}{(\pi D)^2}\bar{h}\left(\frac{180}{\pi D}x, \frac{180}{\pi D}y\right), \\ &= \frac{180^2}{(\pi D)^2}\bar{h}(\bar{x},\bar{y}) = \frac{180^2}{(\pi D)^2}\mathcal{F}^{-1}\{\bar{H}(\bar{u},\bar{v})\}. \quad (7)\end{aligned}$$

In Section II-B, we shall see that the mean squared error depends only on $\tilde{p}(x,y)$ through its autocorrelation function

$$c_{\tilde{p}\tilde{p}}(x,y) = \iint \tilde{p}(s,t)\tilde{p}(s+x, t+y)\, ds\, dt \quad (8)$$

evaluated at points in the printer lattice. That is, the mean squared error depends only on $c_{\tilde{p}\tilde{p}}[m,n] = c_{\tilde{p}\tilde{p}}(mX, nY)$. Assuming a printer with resolution R dpi and a square lattice of addressable points, we find that

$$\begin{aligned}&c_{\tilde{p}\tilde{p}}[m,n] \\ &\quad= \frac{180^2}{(\pi D)^2}\iint \bar{h}(s,t)\bar{h}\left(s + \frac{180m}{\pi RD}, t + \frac{180n}{\pi RD}\right) ds\, dt, \\ &\quad= \frac{180^2}{(\pi D)^2} c_{\bar{h}\bar{h}}\left(\frac{180m}{\pi RD}, \frac{180n}{\pi RD}\right). \quad (9)\end{aligned}$$

We refer to the term $S \equiv RD$ in above equation as the *scale parameter*. We shall see that it plays a very important role in the visual quality of model-based halftoning algorithms. Mathematically, S has the dimension of dots. However, it may be interpreted as the number of dots/radian subtended at the retina when viewing a page printed at resolution R from a distance D. Throughout this paper, we shall use a value of $S = 9.5$ in $\times$ 300 dpi, unless stated otherwise.

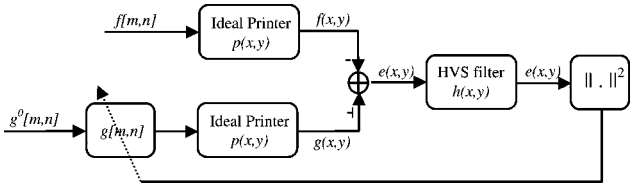

Fig. 1. Block diagram for direct binary search algorithm.

B. Direct Binary Search (DBS) and Error Metric

DBS is an iterative halftoning algorithm which minimizes the error between the perceived continuous-tone image and the perceived halftone image by changing the state of the halftone pixels. Fig. 1 shows a block diagram of the overall algorithm.

The perceived error between the continuous-tone image and the halftone image is given by

$$\tilde{e}(x,y) = \tilde{g}(x,y) - \tilde{f}(x,y) \quad (10)$$

and the mean squared error is given by [24]

$$\mathcal{E} = \sum_{m,n} e[m,n] c_{\tilde{e}\tilde{p}}[m,n] \quad (11)$$

where

$$e[m,n] = g[m,n] - f[m,n] \quad (12)$$

and

$$c_{\tilde{e}\tilde{p}}[m,n] = e[m,n] ** c_{\tilde{p}\tilde{p}}[m,n]. \quad (13)$$

In DBS, there are two kinds of pixel changes, *toggles* and *swaps*. By *toggle*, we mean that we only change the status of the current pixel from 1 (or 0) to 0 (or 1). By *swap*, we mean that we swap the values of the current pixel and one of its 8 nearest neighbor pixels that has a different value. We can express the changed halftone image $g'[m,n]$ as

$$\begin{aligned}g'[m,n] = g[m,n] &+ a_0\delta[m - m_0, n - n_0] \\ &+ a_1\delta[m - m_1, n - n_1] \quad (14)\end{aligned}$$

where $\delta[m,n] = 1$ if $[m,n] = [0,0]$ and 0 otherwise. For a toggle, $a_0 = -1$ if $g[m_0,n_0]$ is changed from 1 to 0, and $a_0 = 1$ if $g[m_0,n_0]$ is changed from 0 to 1; and $a_1 = 0$. For a swap, $g[m_0,n_0]$ and $g[m_1,n_1]$ swap their values; a_0 is as defined for toggle; and $a_1 = -a_0$. After a toggle or a swap, it can be shown [24] that the change in mean squared error is given by

$$\begin{aligned}\Delta\mathcal{E} = \left(a_0^2 + a_1^2\right) c_{\tilde{p}\tilde{p}}[0,0] &+ 2a_0a_1c_{\tilde{p}\tilde{p}}[m_1 - m_0, n_1 - n_0] \\ &+ 2a_0c_{\tilde{e}\tilde{p}}[m_0,n_0] + 2a_1c_{\tilde{e}\tilde{p}}[m_1,n_1]. \quad (15)\end{aligned}$$

This equation is used by DBS to search for the pixel changes in the halftone image. If $\Delta\mathcal{E} < 0$, the halftone pixel change is profitable in the sense of decreasing the mean squared error, and the change will be accepted. If $\Delta\mathcal{E} > 0$, the halftone pixel change will not be accepted. If a trial change is accepted, then $g[m,n]$ will be changed according to (14), and $c_{\tilde{e}\tilde{p}}[m,n]$ must be updated [24] according to

$$\begin{aligned}c'_{\tilde{e}\tilde{p}}[m,n] = c_{\tilde{e}\tilde{p}}[m,n] &+ a_0c_{\tilde{p}\tilde{p}}[m - m_0, n - n_0] \\ &+ a_1c_{\tilde{p}\tilde{p}}[m - m_1, n - n_1]. \quad (16)\end{aligned}$$

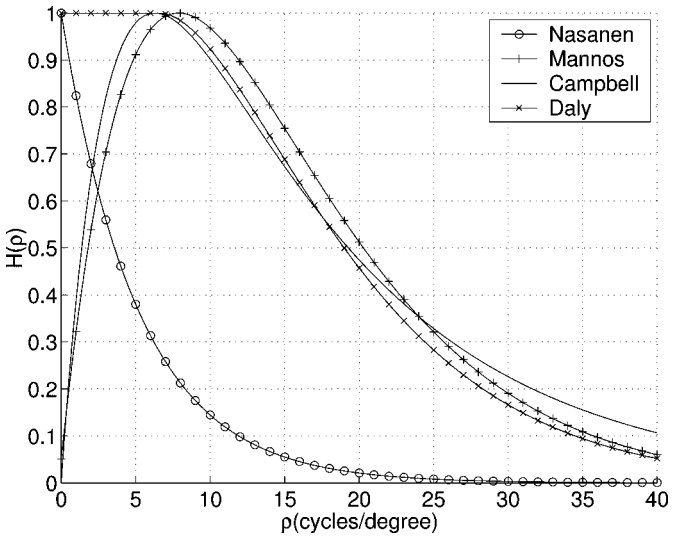

Fig. 2. Contrast sensitivity functions of four HVS models.

If we assume that $c_{\tilde{p}\tilde{p}}[m,n]$ has a support over $N \times N$ pixels, the update (16) requires about N^2 additions. However, the updates are done only when a trial change is accepted according to (15). These are far less common than trial changes, especially after the first few iterations.

III. Human Visual System Models

In this section, we will review five models [26]–[30] that have been proposed in the literature for the CSF of the human visual system. With two exceptions [27] and [30], these models were all developed by measuring viewer responses to simple test patterns, such as sine wave gratings. They have been used in a wide range of image processing and imaging applications. After reviewing the models, we will compare their performance with the DBS halftoning algorithm, and choose one model as the best for use with DBS.

A. Review of HVS Models in the Literature

Campbell *et al.* [26] developed their HVS model by measuring the contrast threshold for detecting sinusoidal interference fringes generated by an oscilloscope at a viewing distance of 57 in. The CSF for this model has a bandpass filter characteristic as shown in Fig. 2. It achieves its maximum at 6.29 cycles/degree. Mannos and Sakrison [27] developed their HVS model by subjective tests done on images that were optimally encoded with different parameters for the model. The subjective test was performed by nine subjects at a viewing distance of 36 in. The resulting CSF also has a bandpass characteristic. It achieves its maximum at 7.9 cycles/degree.

Näsänen's model [28] has a low-pass filter characteristic. Hence, the maximum for the CSF occurs at 0 cycles/degree. In his experiment, vertical gratings were presented for one second at a distance of 256 cm. Daly's HVS model [29] also has a low-pass characteristic. He obtained his model from unpublished empirical data. His model is of the same form as that of Mannos and Sakrison except that he used different parameters; and his model was constructed to be low-pass by extending the maximum point of the exponential function back to the origin of the frequency axis as shown in Fig. 2. The maximum of his CSF occurs at 6.6 cycles/degree.

Barten's model [30] is the most general among the five HVS models reviewed in this paper. Consequently, it can be matched to other HVS models by adjusting its parameters. To develop this model, Barten assumed that the contrast threshold is completely determined by the response of the eye to external noise. He gave several parameter sets which yield CSF curves that match the HVS models he reviewed in his paper. However, he conducted no experiments on his own for developing his model, and hence did not report his own parameter set in [30]. For this reason, we will not include his model in the performance comparison of the HVS models in the following section.

B. Halftoning Results for the HVS Models

In Section II, we showed that the error metric for DBS depends on the HVS model PSF only through samples of its autocorrelation $c_{\bar{h}\bar{h}}(\bar{x},\bar{y})$ taken at interval $180/(\pi S)$ as in (9), where S is the scale parameter given by the product of the viewing distance and printer resolution. The scale parameter has a significant effect on halftone texture, as can be seen in Fig. 3 which shows a short gray ramp halftoned with DBS under Näsänen's model, using three different values for the scale parameter. When the scale parameter is small, the autocorrelation is sparsely sampled; and the sampled autocorrelation $c_{\tilde{p}\tilde{p}}[m,n]$ is nonzero only over a few pixels. In this case, the halftone textures are very fine, but lack homogeneity. As the scale parameter increases, the sampling interval decreases; and the support of $c_{\tilde{p}\tilde{p}}[m,n]$ grows larger. In this case, the error metric averages the halftone textures over a larger window. As a result, DBS creates textures that are coarser, but more homogeneous. Thus we see that for any fixed HVS model, we can create textures with different qualities by simply changing the scale parameter. While in theory, the scale parameter should be determined precisely by the intended viewing distance and printer resolution, it in reality serves more as a free parameter that can be adjusted to yield halftone texture of the desired quality. The choice of value for S is largely based on subjective assessment of how pleasing overall are the halftone textures.

The four HVS models that we described in the preceding section are all expressed in terms of cycles per degree subtended at the retina. Thus, they should, in principle, yield comparable textures for the same value of the scale parameter S. It is evident, however, from Fig. 2 that the models differ widely in terms of bandwidth, and thus support of the sampled autocorrelation $c_{\tilde{p}\tilde{p}}[m,n]$. This disparity is somewhat surprising, although differences in stimuli, viewing conditions, and experimental design under which the models were obtained may partially account for it. Indeed, when we use DBS to generate halftones under the four models as shown in Fig. 2, we see a large variation in texture quality on a range from fine to coarse. However, we can achieve this variation with a single HVS model by simply changing the scale parameter S, as shown in Fig. 3. Our goal instead is to determine the overall texture quality for each HVS model—independent of the scale of the texture. Thus we need some way to normalize the HVS models; so that they all yield textures with a comparable scale. In this paper, we chose to scale the frequency

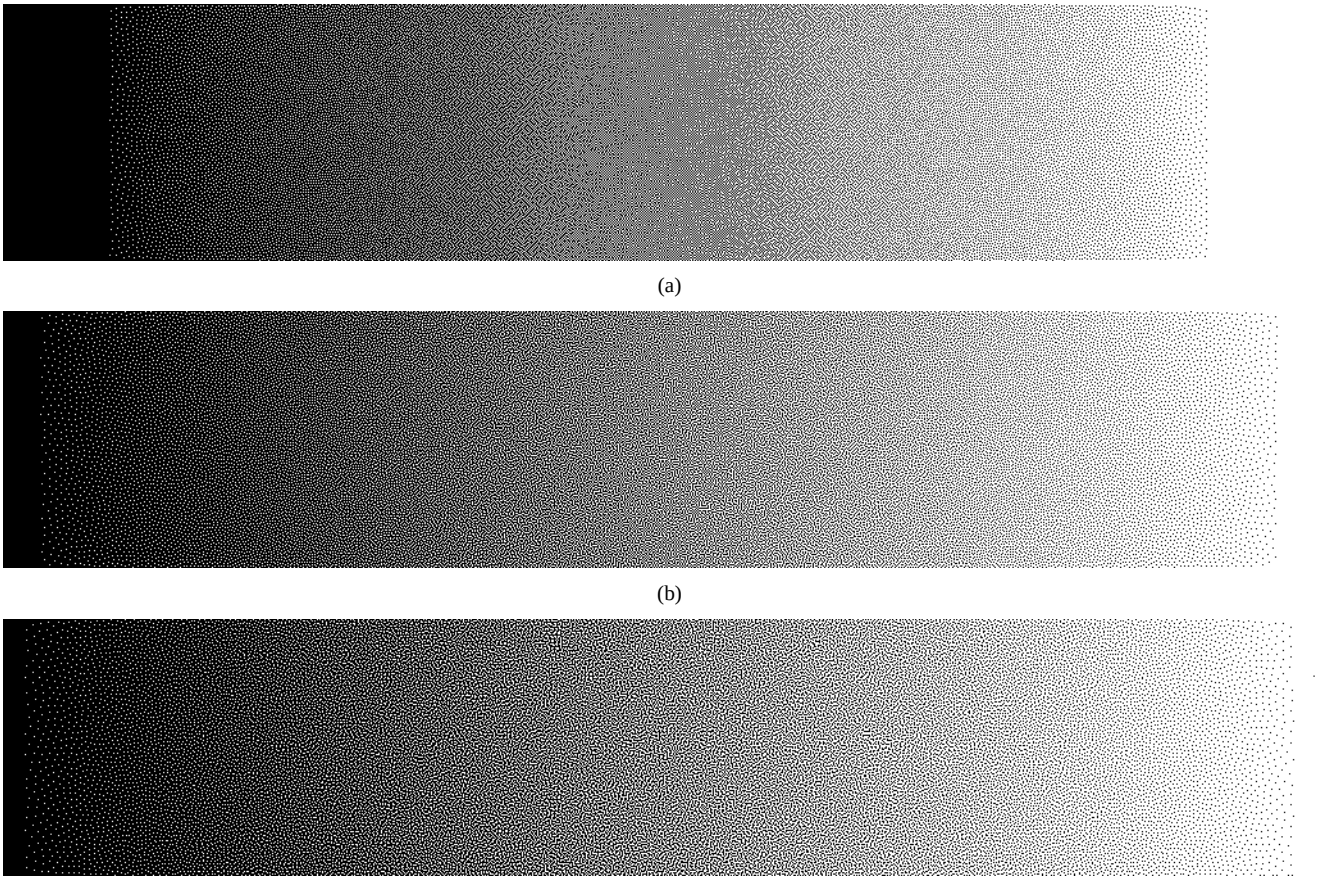

(a) (b) (c)

Fig. 3. Effect of changing the scale parameter $S = 9.5 \times 300$ dots: (a) $S_1 = 0.5S$, (b) $S_2 = S$, and (c) $S_3 = 2S$, printed at 150 dpi.

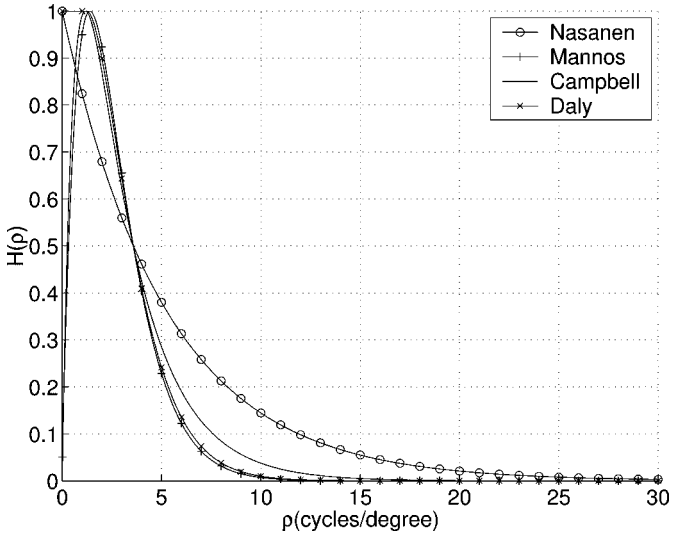

Fig. 4. Scaled contrast sensitivity functions of the four HVS models shown in Fig. 2.

axis of each model so that $\bar{H}(\bar{\rho}_c^N) = 0.5$, where $\bar{\rho}_c^N = 3.58$ cycles/degree is the 50% point for Näsänen's model. Fig. 4 shows the contrast sensitivity functions for the four HVS models after scaling in this manner.

Using each scaled CSF for the HVS model in the DBS algorithm, we obtained the halftone results shown in Fig. 5. We observe that each model has strong points and weak points relative to the three other models. For example, Näsänen's model produces a more smooth halftone image than Campbell's model. But Campbell's model produces a more homogeneous texture in midtone areas than Näsänen's model. This made our choice of one out of the four HVS models difficult. However, we felt that Näsänen's model generally produced halftone images with the best subjective quality. In fact, this observation is consistent with Alford and Mitsa's observation on HVS models. In [31], they found that a low-pass visual model produces better quality halftones than a band-pass model. Therefore, throughout this paper, we will use Näsänen's HVS model as our reference model.

IV. Approximation of HVS Model and Parameter Search

The DBS algorithm consists of three major phases [23]:

1) generation of the initial halftone image;
2) initialization of the table $c_{\tilde{e}\tilde{p}}$;
3) an iterative search for a halftone image that minimizes the error metric given by (11).

The initial halftone can be generated by thresholding with a screen, and thus requires only one operation per pixel. Initialization of the $c_{\tilde{e}\tilde{p}}$ table requires that the entire error image be convolved with the autocorrelation $c_{\tilde{p}\tilde{p}}$, which, typically contains 25×25 pixels.

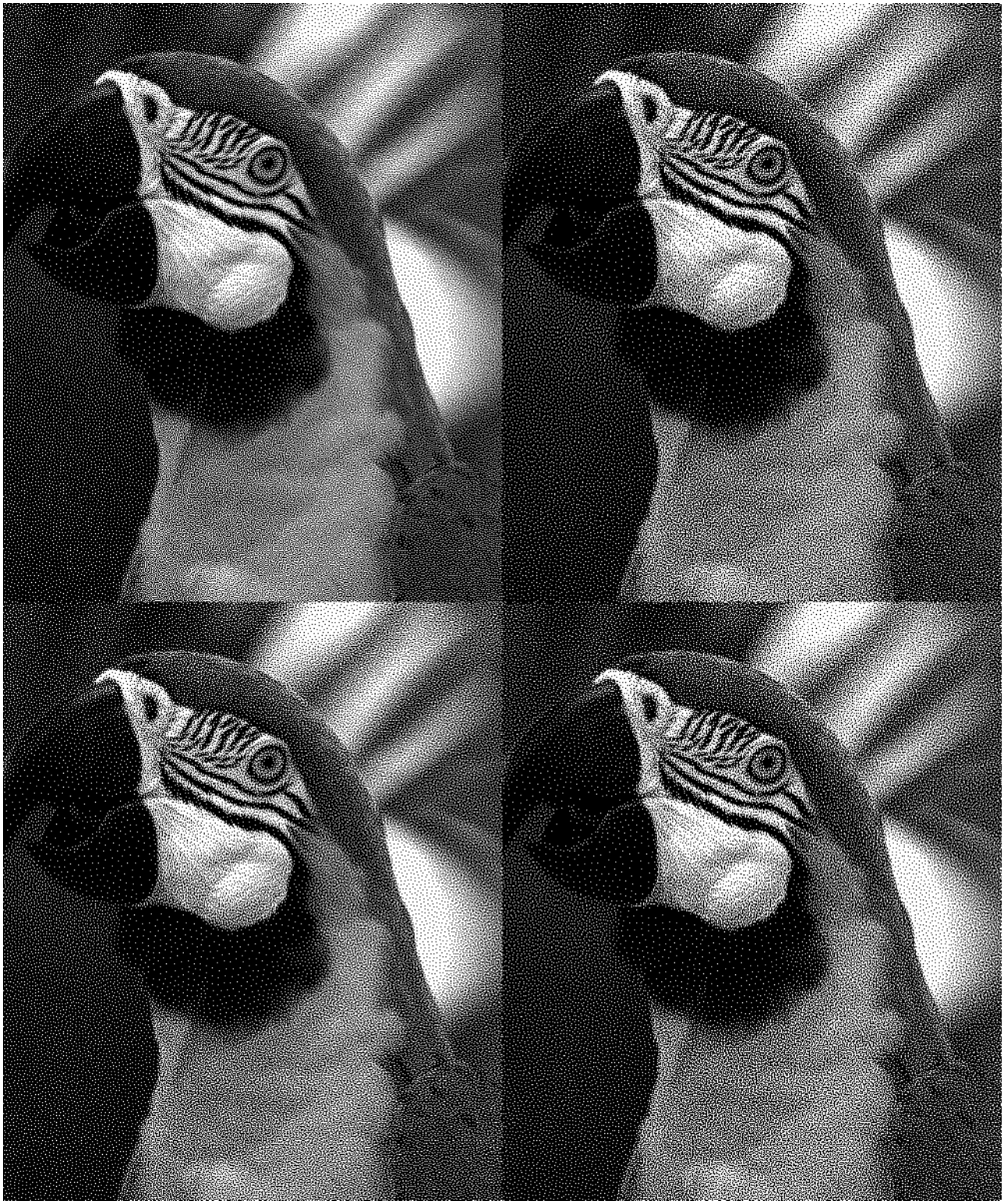

Fig. 5. Halftone results for four different human visual system models: (a) Näsänen, (b) Daly, (c) Mannos, and (d) Campbell, clockwise from left upper, printed at 150 dpi.

We would expect phase 3, the iterative search, to be the most computationally demanding part of DBS. However, with the use of a DBS-designed screen to generate the initial halftone, restricting the swap search to a causal neighborhood of the pixel under consideration, and accepting only one change per 4×5 cell of pixels, Lieberman and Allebach [23] were able to reduce the cost of this part of the algorithm by almost a factor of 30, after which it only represented 33% of the total cost of the DBS computation.

At this point, it was apparent that significant further improvement in the computational performance of DBS rested with decreasing the cost of stage 2. To do this, they approximated the

function $c_{\tilde{p}\tilde{p}}$ as a sum of convolutions of rect functions and rotated rect functions. The improvement in computational efficiency derives from the fact that any 2-D signal may be convolved with an arbitrarily large rect function at a cost of five additions per output point. Although this implementation did reduce the cost of phase 2 by almost a factor of 7, the gain was achieved at the cost of an enormous increase in complexity of the code.

In this section, we consider a different approach to reduce the computational cost of phase 2. In particular, we approximate $c_{\tilde{p}\tilde{p}}$ by a summation of $N \times N$ terms that are separable in $[m, n]$. In this case, the convolution needed to generate $c_{\tilde{c}\tilde{p}}$ will require only $2N$ operations per term in the approximation, instead of the N^2 operations needed overall for convolution with a general 2-D $c_{\tilde{p}\tilde{p}}$.

Since the HVS model that we wish to approximate is circularly symmetric, we chose Gaussian functions which are both separable and circularly symmetric for our approximating terms in the summation. In addition, the Gaussian function has the advantage of being unimodal and smooth, and having a simple closed form Fourier transform. The last property will be important for establishing parameter values in the approximation.

We found that a single Gaussian function could not yield a sufficiently accurate approximation to the autocorrelation $c_{\bar{h}\bar{h}}$ corresponding to Näsänen's model; so we chose the two-component approximation given by

$$\hat{c}_{\bar{h}\bar{h}}(\bar{x}, \bar{y}) = \kappa_1 e^{-(\bar{x}^2+\bar{y}^2)/2\sigma_1^2} + \kappa_2 e^{-(\bar{x}^2+\bar{y}^2)/2\sigma_2^2}. \quad (17)$$

From (5) and the Fourier transform property for correlation, this is equivalent to the squared CSF of the HVS in the frequency domain

$$\hat{\bar{H}}(\bar{u}, \bar{v})^2 = 2\pi\kappa_1\sigma_1^2 e^{-2\pi^2\sigma_1^2\bar{\rho}^2} + 2\pi\kappa_2\sigma_2^2 e^{-2\pi^2\sigma_2^2\bar{\rho}^2}. \quad (18)$$

We performed an exhaustive search for the parameters κ_1, κ_2, σ_1, and σ_2 to minimize the normalized mean squared error in the frequency domain

$$\mathcal{E}_{\hat{\bar{H}}}(\kappa_1, \kappa_2, \sigma_1, \sigma_2) = \frac{\sum_{m,n}(\hat{\bar{H}}[m,n]^2 - \bar{H}[m,n]^2)^2}{\sum_{m,n}\bar{H}[m,n]^4} \quad (19)$$

between the samples of our approximated $\hat{\bar{H}}(\bar{u}, \bar{v})^2$ and the original $\bar{H}(\bar{u}, \bar{v})^2$ from Näsänen's model.

The obtained parameter values are $(\kappa_1^N, \kappa_2^N, \sigma_1^N, \sigma_2^N) = (40.8, 9.03, 0.0384, 0.105)$. With these parameters, we achieved a normalized MSE of 3.0×10^{-3}. Once these parameter values are obtained, we can get the approximated autocorrelation $\hat{c}_{\tilde{p}\tilde{p}}$ of the HVS PSF from (9). In terms of computational cost, using an HP755 workstation to initialize $c_{\tilde{c}\tilde{p}}$ for a 4800×6000 image required 1348 s for direct 2-D convolution, 234 s for separable 2-D convolution using our two-component Gaussian model, and 113 s for 2-D convolution via the rect approximation reported in [23]. Thus we achieved an enormous reduction in code complexity at the cost of a $2\times$ increase in computation. Fig. 6 shows the original $\bar{H}^2$, the approximated $\hat{\bar{H}}^2$, and the approximation error $(\hat{\bar{H}}^2 - \bar{H}^2)$.

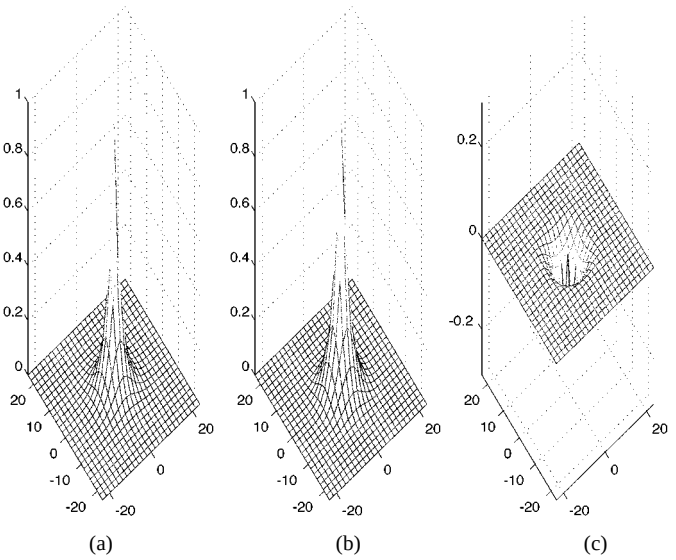

Fig. 6. Approximation of $\bar{H}(\bar{u}, \bar{v})^2$ for (a) Näsänen's model (b) by two-component Gaussian model, and (c) approximation error.

When we compared the halftone image quality achieved with the original $c_{\tilde{p}\tilde{p}}$ and the approximated $\hat{c}_{\tilde{p}\tilde{p}}$, we found surprisingly enough that the image from the approximated $\hat{c}_{\tilde{p}\tilde{p}}$ had slightly more homogeneous texture than the image from the original $c_{\tilde{p}\tilde{p}}$ in most regions. The results of this comparison suggested that there might exist a set of parameters $\kappa_1, \kappa_2, \sigma_1$, and σ_2 that would yield still better image quality.

To find a better human visual model, we first explored a range of bandwidths for our approximated CSF model in (18) since the bandwidth of a HVS CSF has a huge impact on the texture quality of the resulting halftone as we discussed in Section III-B. To obtain the bandwidth which yields the visually optimal halftone, we gradually increased or decreased the cutoff frequency $\bar{\rho}_c$ of our approximated CSF by scaling the frequency axis, while keeping $(\kappa_1, \kappa_2, \sigma_1, \sigma_2) = (\kappa_1^N, \kappa_2^N, \sigma_1^N, \sigma_2^N)$ constant, and evaluated the resulting halftone images. As before, the cutoff frequency $\bar{\rho}_c$ is the frequency where the magnitude of the CSF falls to the half of its maximum height. Visual assessment of the halftone images corresponding to the different values for $\bar{\rho}_c$ suggested that $\bar{\rho}_c^* = 1.4\bar{\rho}_c^N$ is the best value for the DBS algorithm, where as before $\bar{\rho}_c^N = 3.58$ cycles/degree is the cutoff frequency of Näsänen's model.

To further refine the parameters of the visual model (18), we next explored a range of values for $(\kappa_1, \kappa_2, \sigma_1, \sigma_2)$, subject to some constraints. If we set $\alpha = \kappa_2\sigma_2^2/\kappa_1\sigma_1^2$ and $\sigma_2 = \beta\sigma_1$, (18) can be rewritten as

$$\hat{\bar{H}}(\bar{u}, \bar{v})^2 = 2\pi\kappa_1\sigma_1^2\left(e^{-2\pi^2\sigma_1^2\bar{\rho}^2} + \alpha e^{-2\pi^2\beta^2\sigma_1^2\bar{\rho}^2}\right). \quad (20)$$

This function must satisfy the following two constraints:

$$\hat{\bar{H}}(0,0) = 1 \quad (21)$$

$$\hat{\bar{H}}(\bar{u}, \bar{v}) = 0.5 \quad \text{for } \sqrt{\bar{u}^2 + \bar{v}^2} = \bar{\rho}_c^* \quad (22)$$

where $\bar{\rho}_c^* = 1.4\bar{\rho}_c^N = 5.012$ cycles/degree is the optimal cutoff frequency we obtained in the previous step of the search. Equa-

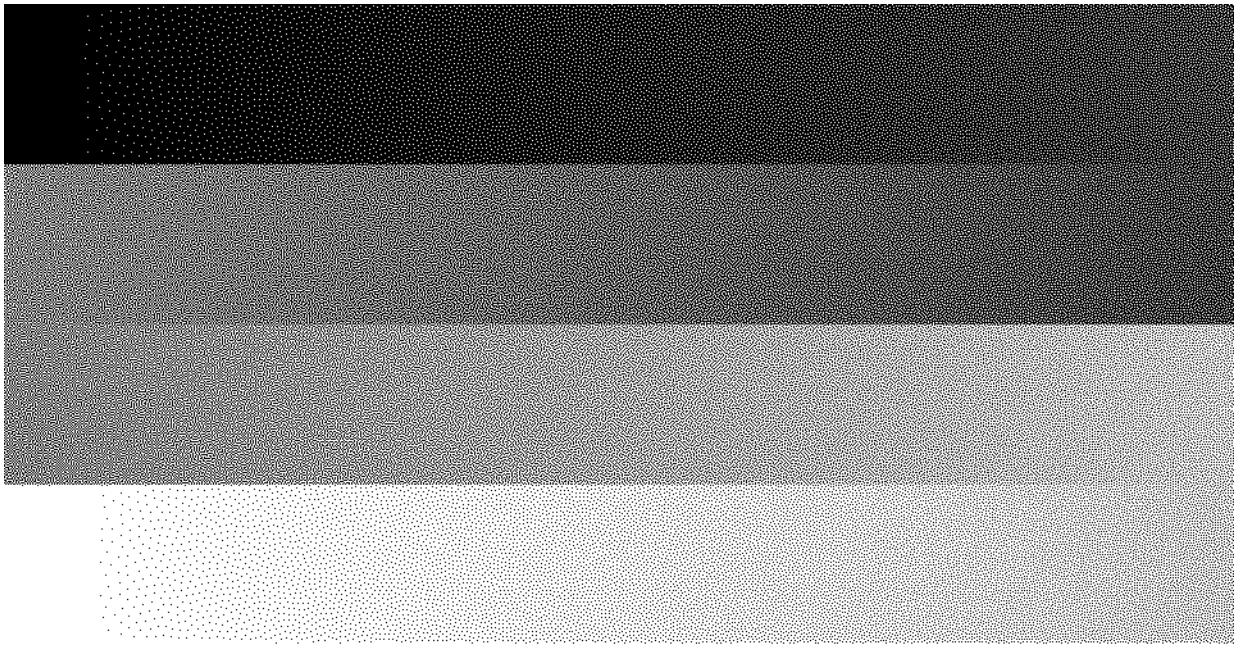

(a)

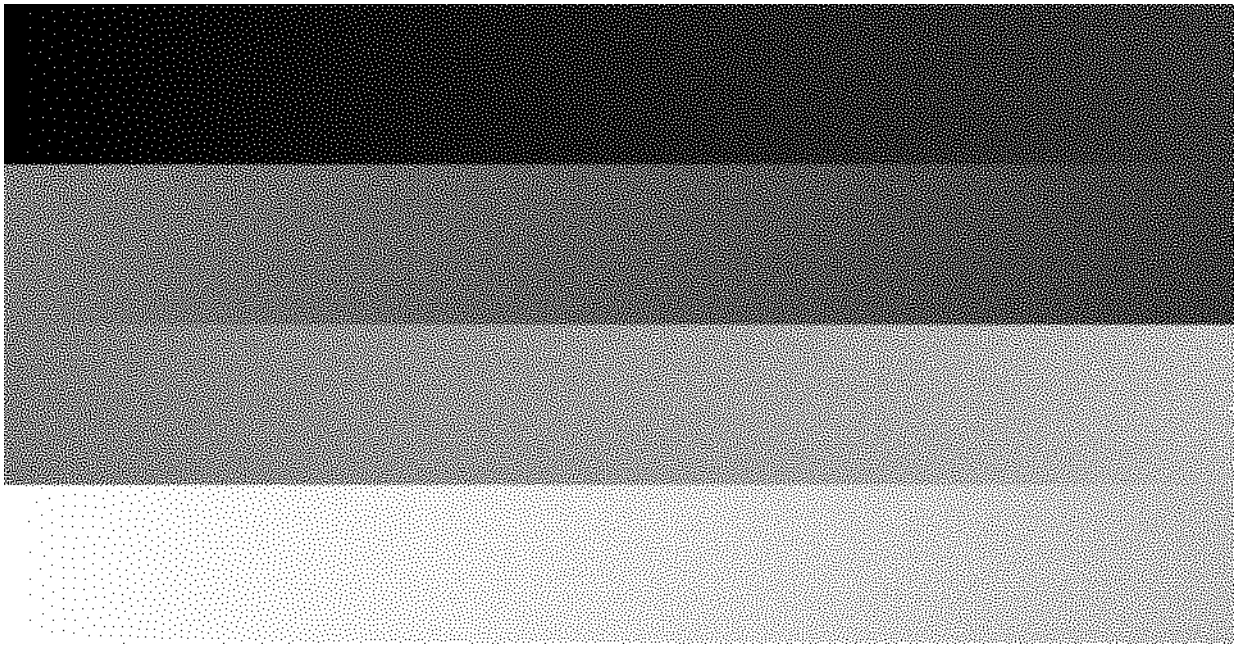

(b)

Fig. 7. Ramp image generated with the two-component Gaussian model with (a) $(\alpha, \beta) = (6.65, 2.73)$ and (b) $(\alpha, \beta) = (6.65, 1.73)$.

tion (21) is required to guarantee the preservation of tone. Applying these constraints to (20), we obtain

$$\kappa_1 = \frac{1}{2\pi\sigma_1^2(1+\alpha)} \tag{23}$$

$$\frac{1}{1+\alpha}e^{-2\pi^2\sigma_1^2\bar{\rho}_c^{*2}} + \frac{\alpha}{1+\alpha}e^{-2\pi^2\sigma_1^2\beta^2\bar{\rho}_c^{*2}} = 0.25. \tag{24}$$

Since the constraints remove two out of the four degrees of freedom in the parameter space of $c_{\tilde{p}\tilde{p}}(x, y)$, we will have a unique solution of $(\kappa_1, \kappa_2, \sigma_1, \sigma_2)$ for each fixed (α, β). To solve for $(\kappa_1, \kappa_2, \sigma_1, \sigma_2)$ for a fixed (α, β), we obtain σ_1 by solving (24), solve for κ_1 from (23) using the obtained σ_1, get σ_2 from the relationship $\sigma_2 = \beta\sigma_1$, then get κ_2 from the relationship $\alpha = \kappa_2\sigma_2^2/\kappa_1\sigma_1^2$.

To find a visually optimal parameter set (α^*, β^*) or equivalently $(\kappa_1^*, \kappa_2^*, \sigma_1^*, \sigma_2^*)$, we perturbed (α^N, β^N) to get a new set of values $(\alpha, \beta) = (\alpha^N + \Delta\alpha, \beta^N + \Delta\beta)$, where $(\alpha^N, \beta^N) = (1.65, 2.73)$ are the values for $(\kappa_1^N, \kappa_2^N, \sigma_1^N, \sigma_2^N)$. The perturbation amounts $(\Delta\alpha, \Delta\beta)$ were chosen empirically to yield a sufficiently fine sampling of the parameter space, while allowing exploration of a large enough range over that space to show significant differences in texture quality. We examined over forty different combinations of (α, β), and for each (α, β) combination, we halftoned and printed a full page ramp at 150 dpi. We compared these pages side by side from a range of viewing

distances and evaluated the halftone textures with respect to smoothness, uniformity, and freedom from artifacts.

Unfortunately, we could not select a single set (α_0, β_0) which works best for every level of tone. Instead, for every (α, β) pair, we see a tradeoff between the homogeneity and the smoothness of the texture. For example, the set (6.65, 2.73) produces Fig. 7(a) which has smoother texture than Fig. 7(b) from the set (6.65, 1.73); but (6.65, 1.73) produces a more homogeneous texture than (6.65, 2.73), especially in the midtone areas. This phenomenon motivates the dual-metric DBS which will be presented in the next section.

V. Dual-Metric DBS Halftone Algorithm

A. Dual-Metric DBS

Since we did not observe a single parameter set for our two-component Gaussian HVS model that worked best for all levels of tone, we considered making the HVS model tone-dependent. Thus, our new HVS point spread function $h(x, y; f(x, y))$ would depend on the value of the continuous-tone image at each point (x, y). This was done previously in [8], [22], [32], [33], and [34]. However, as shown in [22], this significantly increases both the computation and storage required for DBS. To achieve a result similar to that provided by a tone-dependent HVS model while minimizing the increase in computational complexity, we then considered using a mixture model in which we effectively combine two fixed HVS models with relative weights that are tone-dependent. There are a number of ways in which this can be done. For example, we could use two different point spread functions h_1 and h_2 in a tone-dependent mixture. However, this will also have a serious negative impact on the computational efficiency of DBS. Instead we define a new dual-component error metric

$$\mathcal{E} = \sum_{i=1}^{2} \int\int |\tilde{e}_i(x, y)|^2 \, dx \, dy \tag{25}$$

where

$$\tilde{e}_i(x, y) = \{w_i(f(x, y))[g(x, y) - f(x, y)]\} ** h_i(x, y). \tag{26}$$

Let us assume that $w_i(f(x, y))[g(x, y) - f(x, y)]$ can be expressed in terms of its sample values as the output of an ideal printer in the form shown in (1) and (2). Then, following the same steps indicated in (3), (4) and (10), (11) we obtain

$$\mathcal{E} = \sum_{i=1}^{2} \sum_{m,n} \sum_{k,l} e_i[m, n] e_i[k, l] c_{\tilde{p}_i \tilde{p}_i}[m - k, n - l] \tag{27}$$

where

$$e_i[m, n] = w_i[f[m, n]](g[m, n] - f[m, n]). \tag{28}$$

Here, $w_i[f[m, n]], i = 1, 2$ are tone-dependent weights; and $c_{\tilde{p}_i \tilde{p}_i}, i = 1, 2$ are the two HVS models used in the dual-metric DBS. For $c_{\tilde{p}_1 \tilde{p}_1}$, we use $(\alpha, \beta) = (6.65, 2.73)$. For $c_{\tilde{p}_2 \tilde{p}_2}$, we use $(\alpha, \beta) = (6.65, 1.73)$.

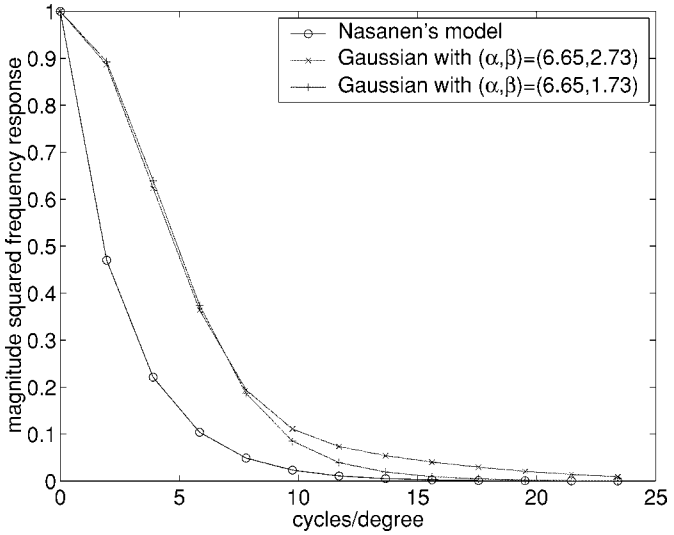

(a)

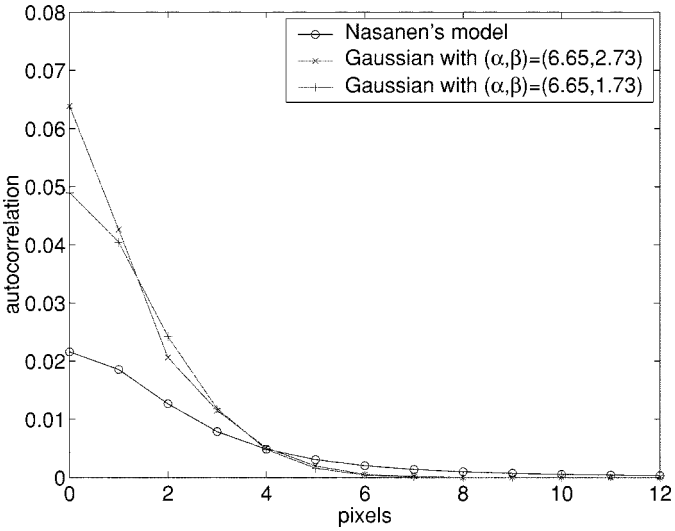

(b)

Fig. 8. Selected two-component Gaussian visual models: (a) $\hat{\tilde{H}}(\bar{\rho})^2$ and (b) $c_{\tilde{p}\tilde{p}}[m, n]$.

We selected (6.65, 2.73) and (6.65, 1.73) as our two parameter sets, because we found that they visually complement each other. The HVS model with (6.65, 2.73) produces a very smooth halftone result overall, but generates patchy texture in midtone areas. It also results in clipping [22] at extreme tone levels. In contrast, the HVS model with (6.65, 1.73) generates good results in midtone areas and in areas of extreme tone. So, they will complement each other in the dual-metric algorithm, and produce excellent halftone texture across the entire range of the tone scale. The complete models for parameter sets $(\alpha, \beta) = (6.65, 2.73)$ and $(6.65, 1.73)$, which corresponds to $(\kappa_1, \kappa_2, \sigma_1, \sigma_2) = (43.2, 38.7, 0.0219, 0.0598)$ and $(19.1, 42.7, 0.0330, 0.0569)$, respectively, are illustrated in Fig. 8. The original Näsänen's model is also included in Fig. 8 for comparison.

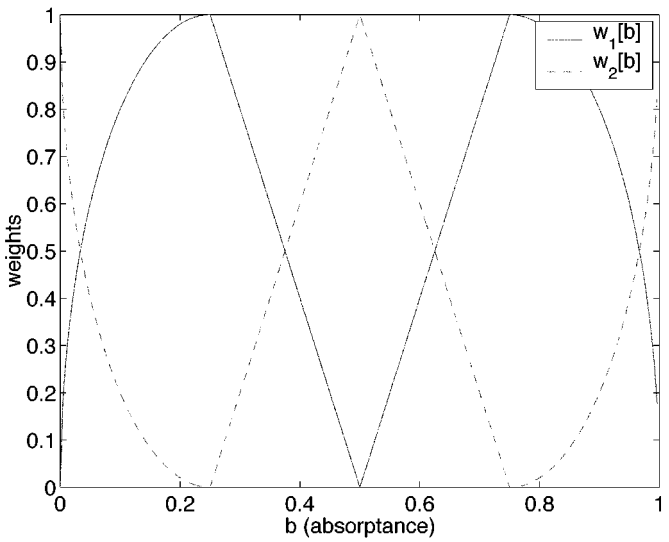

Fig. 9. Tone-dependent weights for dual-metric DBS.

The weights $w_i[b]$ play a crucial role in our dual-metric DBS, since they determine the quality of the resulting halftone images. In this paper, we used the tone-dependent weights shown in Fig. 9. To design the weights in Fig. 9, we considered some properties that they should have. First, the weights should satisfy $w_1[b] + w_2[b] = 1$ for every possible value of absorptance b. Second, they should be a continuous function of tone to prevent an abrupt change in the texture characteristics. Finally, we prefer $\tilde{p}_2$ in extreme and midtone levels; and we prefer $\tilde{p}_1$ in the absorptance ranges $(1/8, 1/4)$ and $(3/4, 7/8)$. Thus, we have

$$w_1[b] = \begin{cases} \sqrt{1-(4b-1)^2}, & 0 \le b < 0.25, \\ |4b-2|, & 0.25 \le b < 0.75, \\ \sqrt{1-(4b-3)^2}, & 0.75 \le b < 1, \end{cases} \quad (29)$$

$$w_2[b] = 1 - w_1[b]. \quad (30)$$

Note that $w_1[b]$ climbs up to its maximum value very fast due to the elliptical equation in (30) between the absorptance ranges $(0, 1/4)$. This is because we prefer $\tilde{p}_1$ for most of the levels in $(0, 1/4)$ except some extreme levels. The same logic applies to the absorptance ranges $(3/4, 1)$. However, in the ranges $(1/4, 3/4)$, we found by visual assessment of halftone images that a linear ramp for $w_1[b]$ works better than the arched shape.

B. Efficient Implementation for Dual-Metric DBS

In this section, we show that for dual-metric DBS, the effect of a toggle or a swap can be evaluated in an efficient manner that is analogous to that for standard DBS. Consider again the change in the halftone image induced by a toggle or a swap as represented by (14). Substituting this expression into (28), we see that the new error is given by

$$e_i'[m,n] = e_i[m,n] + a_0 w_i[f[m_0,n_0]]\delta[m-m_0, n-n_0] + a_1 w_i[f[m_1,n_1]]\delta[m-m_1, n-n_1]. \quad (31)$$

Then, substituting (31) into (27), we find that the new value for the error metric is given by

$$\begin{aligned}
\mathcal{E}' &= \sum_{i=1}^{2} \sum_{m,n} \sum_{k,l} e_i'[m,n] e_i'[k,l] c_{\tilde{p}_i\tilde{p}_i}[m-k, n-l], \\
&= \mathcal{E} + \sum_{i=1}^{2} \Bigg[\left(a_0^2 w_i^2[f[m_0,n_0]] + a_1^2 w_i^2[f[m_1,n_1]]\right) \\
&\quad \times c_{\tilde{p}_i\tilde{p}_i}[0,0] + 2a_0 w_i[f[m_0,n_0]] a_1 w_i[f[m_1,n_1]] \\
&\quad \times c_{\tilde{p}_i\tilde{p}_i}[m_0-m_1, n_0-n_1] \\
&\quad + 2a_0 w_i[f[m_0,n_0]] \sum_{k,l} e_i[k,l] c_{\tilde{p}_i\tilde{p}_i}[m_0-k, n_0-l] \\
&\quad + 2a_1 w_i[f[m_1,n_1]] \sum_{k,l} e_i[k,l] c_{\tilde{p}_i\tilde{p}_i}[m_1-k, n_1-l] \Bigg], \\
&= \mathcal{E} + \sum_{i=1}^{2} \left[\left(a_0^2 w_i^2[f[m_0,n_0]] + a_1^2 w_i^2[f[m_1,n_1]]\right) \right. \\
&\quad \times c_{\tilde{p}_i\tilde{p}_i}[0,0] + 2a_0 w_i[f[m_0,n_0]] a_1 w_i[f[m_1,n_1]] \\
&\quad \times c_{\tilde{p}_i\tilde{p}_i}[m_0-m_1, n_0-n_1] \\
&\quad + 2a_0 w_i[f[m_0,n_0]] c_{\tilde{e}_i\tilde{p}_i}[m_0,n_0] \\
&\quad \left. + 2a_1 w_i[f[m_1,n_1]] c_{\tilde{e}_i\tilde{p}_i}[m_1,n_1] \right] \quad (32)
\end{aligned}$$

where we have used the definition for $c_{\tilde{e}\tilde{p}}[m,n]$ given by (13). Hence, the change in the error metric is given by

$$\begin{aligned}
\Delta\mathcal{E} &= \mathcal{E}' - \mathcal{E}, \\
&= \sum_{i=1}^{2} \left[\left(a_0^2 w_i^2[f[m_0,n_0]] + a_1^2 w_i^2[f[m_1,n_1]]\right) c_{\tilde{p}_i\tilde{p}_i}[0,0] \right. \\
&\quad + 2a_0 w_i[f[m_0,n_0]] a_1 w_i[f[m_1,n_1]] \\
&\quad \times c_{\tilde{p}_i\tilde{p}_i}[m_0-m_1, n_0-n_1] \\
&\quad + 2a_0 w_i[f[m_0,n_0]] c_{\tilde{e}_i\tilde{p}_i}[m_0,n_0] \\
&\quad \left. + 2a_1 w_i[f[m_1,n_1]] c_{\tilde{e}_i\tilde{p}_i}[m_1,n_1] \right]. \quad (33)
\end{aligned}$$

Comparing (33) with (15), we see that the computational structure for evaluating the effect of a trial change with dual-metric DBS is similar to that for standard DBS. Although (33) requires significantly more computation than (15), it is still about two orders of magnitude less than direct evaluation of the effect of a trial change. Note that all the terms involving the weights $w_i[f[m,n]], i = 1,2$ or products of these weights may be precomputed and stored. These tables will be the size of the entire image or a block from the image in a block-based implementation [23]. As with standard DBS, the functions $c_{\tilde{e}_i\tilde{p}_i}[m,n], i = 1,2$ must be updated whenever a trial change is accepted. For the dual-metric DBS, the update equation is given by

$$\begin{aligned}
&c_{\tilde{e}_i\tilde{p}_i}'[m,n] \\
&\quad = \sum_{k,l} e_i'[k,l] c_{\tilde{p}_i\tilde{p}_i}[m-k, n-l], \\
&\quad = c_{\tilde{e}_i\tilde{p}_i}[m,n] + a_0 w_i[f[m_0,n_0]] c_{\tilde{p}_i\tilde{p}_i}[m-m_0, n-n_0] \\
&\qquad + a_1 w_i[f[m_1,n_1]] c_{\tilde{p}_i\tilde{p}_i}[m-m_1, n-n_1] \quad (34)
\end{aligned}$$

which again is very similar to the update equation (16) required for standard DBS.

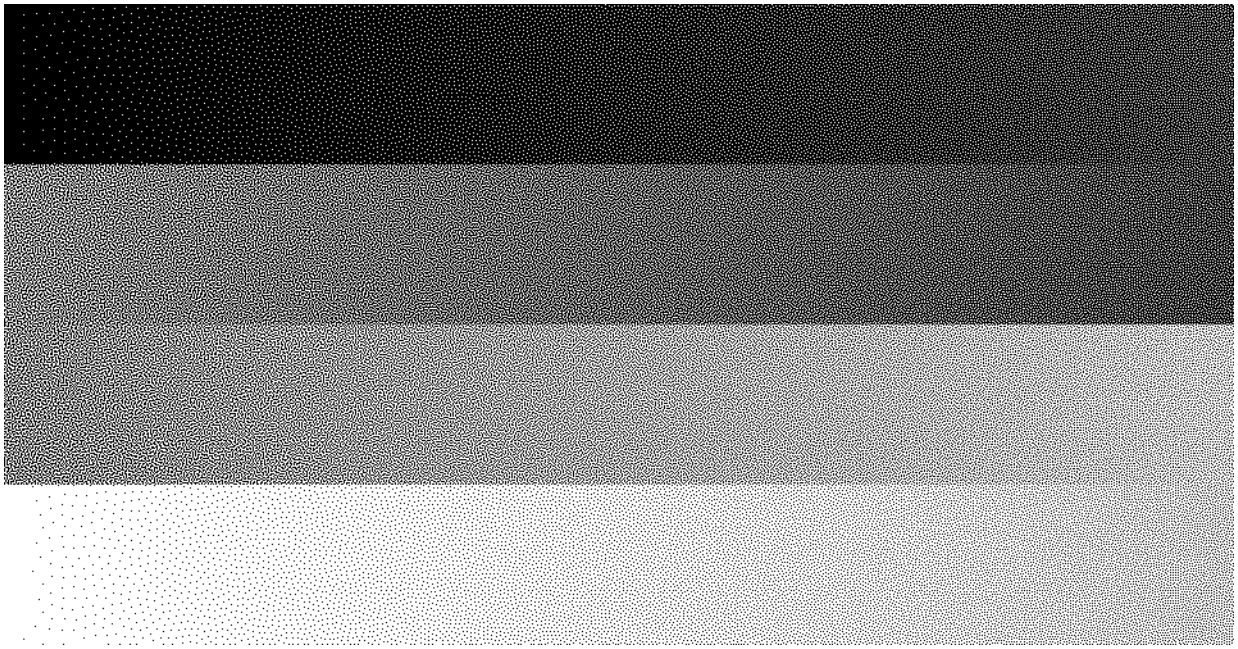

Fig. 10. Ramp image generated by dual-metric DBS.

C. Experimental Results

Fig. 10 shows the performance of dual-metric DBS. As stated earlier, for the dual-metric algorithm, we used $(\alpha, \beta) = (6.65, 2.73)$ and $(6.65, 1.73)$ for our two HVS models, and the weights $w_i[f[m,n]]$ shown in Fig. 9. In Fig. 10, we see that dual-metric DBS yields consistently good results over the whole range of the tone scale, while standard DBS with a fixed HVS model cannot yield consistently good results as shown in Fig. 7(a) and (b). Note that Fig. 10 does not show the clipping in extreme levels and the patchiness in midtone areas that can be seen in Fig. 7(a). Also Fig. 10 has much smoother texture than Fig. 7(b) especially in the quarter-tone areas.

VI. Conclusion

Of the four HVS models that we compared, Näsänen's model yielded the best overall halftone quality when used with the DBS algorithm. A two-component Gaussian model with parameters chosen to give a best fit to Näsänen's model yielded even better halftone quality. This model allows for very efficient initialization of the lookup tables used by DBS, with minimal increase in code complexity. By varying the parameters of the two-component Gaussian model, we found that it could be tuned to provide the best quality at each gray level. The dual-metric DBS algorithm effectively realizes a similar tone-dependent HVS model, while retaining computational efficiency comparable to that of the standard DBS algorithm.

References

[1] B. E. Bayer, "An optimum method for two-level rendition of continuous-tone pictures," *Proc. IEEE Int. Conf. Communications*, vol. 26, pp. 2611–2615, June 11–13, 1973.

[2] J. R. Sullivan, L. A. Ray, and R. Miller, "Design of minimum visual modulation halftone patterns," *IEEE Trans. Syst., Man, Cybern.*, vol. 21, pp. 33–38, Jan. 1991.

[3] R. W. Floyd and L. Steinberg, "An adaptive algorithm for spatial grayscale," *J. Soc. Inform Display*, vol. 17, no. 2, pp. 75–77, 1976.

[4] G. Sharma and H. J. Trussell, "Digital color imaging," *IEEE Trans. Image Processing*, vol. 6, pp. 901–932, July 1997.

[5] J. P. Allebach, Ed., *Selected Papers on Digital Halftoning*. Bellingham, WA: SPIE, 1999.

[6] T. Mitsa and K. J. Parker, "Digital halftoning technique using a blue-noise mask," *J. Opt. Soc. Amer. A*, vol. 9, pp. 1920–1929, Nov. 1992.

[7] J. P. Allebach and Q. Lin, "FM screen design using DBS algorithm," *Proc. IEEE Int. Conf. Image Processing*, vol. 1, pp. 549–552, Sept. 1996.

[8] Q. Lin and J. P. Allebach, "Color FM screen design using DBS algorithm," in *Proc. IS&T/SPIE Int. Symp. on Electronic Imaging Science and Technology*, vol. 3300, San Jose, CA, Jan. 28–30, 1998, pp. 353–361.

[9] D. Kacker and J. P. Allebach, "Aperiodic micro-screen design using DBS and training," in *Proc. IS&T/SPIE Int. Symp. on Electronic Imaging Science and Technology*, vol. 3300, San Jose, CA, Jan. 28–30, 1998, pp. 386–397.

[10] P. Li and J. P. Allebach, "Look-up-table based halftoning algorithm," *IEEE Trans. Image Processing*, vol. 9, pp. 1593–1603, Sept. 2000.

[11] J. P. Allebach, "Human vision and image rendering: Is the story over, or is it just beginning," in *Proc. IS&T/SPIE Int. Symp. on Human Vision and Electronic Imaging III*, vol. 3299, San Jose, CA, Jan. 26–29, 1998, pp. 26–37.

[12] R. Ulichney, *Digital Halftoning*. Cambridge, MA: MIT Press, 1987.

[13] J. R. Sullivan and L. Ray, "Digital halftoning with correlated minimum visual modulation patterns," U.S. Patent 5 214 517, 1993.

[14] B. W. Kolpatzik and C. A. Bouman, "Optimized error diffusion for image display," *J. Elect. Imag.*, vol. 1, no. 3, pp. 277–292, July 1992.

[15] J. Sullivan, R. Miller, and G. Pios, "Image halftoning using a visual model in error diffusion," *J. Opt. Soc. Amer. A*, vol. 10, no. 8, pp. 1714–1724, Aug. 1993.

[16] P. W. Wong, "A mixture distortion criterion for halftones," in *Proc. OSA/IS&T Meeting on Optics and Imaging*, Rochester, NY, Oct. 1996, pp. 187–191.

[17] P. W. Wong and J. P. Allebach, "Optimum error diffusion kernal design," in *Proc. IS&T/SPIE Int. Symp. on Electronic Imaging Science and Technology*, vol. 3018, San Jose, CA, Feb. 10–14, 1997, pp. 236–242.

[18] A. Zakhor, S. Lin, and F. Eskafi, "A new class of b/w and color halftoning algorithms," *IEEE Trans. Image Processing*, vol. 2, pp. 499–509, Oct. 1993.

[19] M. Analoui and J. P. Allebach, "Model-based halftoning using direct binary search," in *Proc. IS&T/SPIE Int. Symp. on Electronic Imaging Science and Technology*, vol. 1666, San Jose, CA, Feb. 9–14, 1992, pp. 96–108.

[20] J. B. Mulligan and A. J. Ahumada Jr., "Principled halftoning based on models of human vision," in *Proc. IS&T/SPIE Int. Symp. on Electronic Imaging Science and Technology*, vol. 1666, San Jose, CA, Feb. 9–14, 1992, pp. 109–121.
[21] T. N. Pappas and D. L. Neuhoff, "Least-squares model-based halftoning," in *Proc. IS&T/SPIE Int. Symp. on Electronic Imaging Science and Technology*, vol. 1666, San Jose, CA, Feb. 9–14, 1992, pp. 165–176.
[22] D. J. Lieberman and J. P. Allebach, "Digital halftoning using the direct binary search algorithm," in *Proc. IS&T 5th Int. Conf. High Tech.*, Chiba, Japan, Sept. 11–14, 1996, pp. 114–124.
[23] ——, "Efficient model based halftoning using direct binary search," *Proc. IEEE Int. Conf. Image Processing*, vol. 1, pp. 775–778, Oct. 26–29, 1997.
[24] ——, "A dual interpretation for direct binary search and its implications for tone reproduction and texture quality," *IEEE Trans. Image Processing*, vol. 9, pp. 1950–1969, Nov. 2000.
[25] B. E. Rogowitz, T. N. Pappas, and J. P. Allebach, "Human vision and electronic imaging," *J. Electron. Imag.*, vol. 10, Jan. 2001.
[26] F. W. Campbell, R. H. S. Carpenter, and J. Z. Levinson, "Visibility of aperiodic patterns compared with that of sinusoidal gratings," *J. Physiol.*, vol. 204, pp. 283–298, 1969.
[27] J. L. Mannos and D. J. Sakrison, "The effects of a visual fidelity criterion on the encoding of images," *IEEE Trans. Inform. Theory*, vol. IT-20, July 1974.
[28] R. Näsänen, "Visibility of halftone dot textures," *IEEE Trans. Syst., Man, Cybern.*, vol. 14, no. 6, pp. 920–924, 1984.
[29] S. Daly, "Subroutine for the Generation of a Two Dimensional Human Visual Contrast Sensitivity Function," Eastman Kodak, Tech. Rep. 233203y, 1987.
[30] P. J. Barten, "Physical model for the contrast sensitivity of the human eye," in *Proc. IS&T/SPIE Int. Symp. on Electronic Imaging Science and Technology*, vol. 1666, San Jose, CA, Feb. 9–14, 1992, pp. 57–72.
[31] J. R. Alford and T. Mitsa, "Qualitative comparison of visual models in an iterative halftoning procedure," *Proc. IEEE Int. Conf. Image Processing*, vol. 2, pp. 339–342, Oct. 23–26, 1995.
[32] R. Eschbach, "Reduction of artifacts in error diffusion by means of input-dependent weights," *J. Electron. Imag.*, vol. 2, pp. 352–358, Oct. 1993.
[33] Q. Lin, "Improving halftone uniformity and tonal response," in *Proc. IS&T's 10th Int. Congr. Adv. in Non-Impact Tech.*, New Orleans, LA, Oct. 30–Nov. 4 1994, pp. 377–380.
[34] H. Nishida, "Adaptive model-based digital halftoning incorporating image enhancement," *Proc. 15th IEEE Int. Conf. Pattern Recogmition*, vol. 3, pp. 306–309, Sept. 3–7, 2000.

Sang Ho Kim (S'97) received the B.S. degree in electrical engineering from Seoul National University, Seoul, Korea, in 1990 and the M.S. degree from Pohang University of Science and Technology, Pohang, Korea, in 1992. He is currently pursuing the Ph.D. degree in the School of Electrical and Computer Engineering, Purdue University, West Lafayette, IN.

From 1992 to 1997, he was a Research Engineer at Daewoo Electric Co., Ltd., Seoul, where he worked on video compression, motion estimation, and pre/postprocessing for HDTV systems. His research interests include electronic imaging systems, color processing, video coding, and image enhancement.

Jan P. Allebach (S'70–M'76–SM'89–F'91) received the B.S.E.E. degree from the University of Delaware, Newark, in 1972 and the Ph.D. degree from Princeton University, Princeton, NJ, in 1976.

He was on the faculty at the University of Delaware from 1976 to 1983. Since 1983, he has been with the School of Electrical and Computer Engineering, Purdue University, West Lafayette, IN. His current research interests include image rendering, image quality, color imaging, and document management. He is Editor for the *Journal of Electronic Imaging*.

Dr. Allebach is active in both the IEEE Signal Processing Society and the Society for Imaging Science and Technology (IS&T). He is a Fellow of both societies, has served as Distinguished/Visiting Lecturer for both societies, and has served as an Officer and on the Board of Directors of both societies. He is a past Associate Editor for the IEEE TRANSACTIONS ON SIGNAL PROCESSING and the IEEE TRANSACTIONS ON IMAGE PROCESSING. He received the Senior (Best Paper) Award from the IEEE Signal Processing Society and the Bowman Award from IS&T.